Monthly Notices of the ROYAL ASTRONOMICAL SOCIETY
MNRAS **441,** 630–639 (2014) doi:10.1093/mnras/stu468

High spatial resolution of the mid-infrared emission of the Compton-thick type 2 Seyfert galaxy, Markarian 3

Dinalva A. Sales,[1,2]★ D. Ruschel-Dutra,[2] M. G. Pastoriza,[2,3] R. Riffel[2] and Cláudia Winge[4]

[1]*Department of Physics, Rochester Institute of Technology, 84 Lomb Memorial Drive, Rochester, NY 14623, USA*
[2]*Departamento de Astronomia, Universidade Federal do Rio Grande do Sul. 9500 Bento Gonçalves, Porto Alegre, 91501-970, Brazil*
[3]*Conselho Nacional de Desenvolvimento Científico e Tecnológico, Brasilia, 71605-001, Brazil*
[4]*Gemini Observatory, c/o Aura, Inc., Casilla 603, La Serena, Chile*

Accepted 2014 March 6. Received 2014 February 21; in original form 2013 November 13

ABSTRACT

The mid-infrared (MIR) spectra observed with Gemini/Michelle have been used to study the nuclear region of the Compton-thick type 2 Seyfert galaxy, Markarian 3 (Mrk 3), at a spatial resolution of ∼200 pc. No polycyclic aromatic hydrocarbon emission bands were detected in the *N*-band spectrum of Mrk 3. However, intense [Ar III] 8.99 μm, [S IV] 10.5 μm and [Ne II] 12.8 μm ionic emission lines, as well as a silicate absorption feature at 9.7 μm, have been found in the nuclear extraction (∼200 pc). We also present a subarcsecond-resolution Michelle *N*-band image of Mrk 3, which resolves its circumnuclear region. This diffuse MIR emission shows up as a wing towards the east–west direction, closely aligned with the S-shape of the narrow-line region observed in the optical [O III] λ5007Å image from the Faint Object Camera onboard the *Hubble Space Telescope*. The nuclear continuum spectrum can be well represented by a theoretical torus spectral energy distribution, suggesting that the nucleus of Mrk 3 might host a dusty toroidal structure, as predicted by the unified model of an active galactic nucleus (AGN). In addition, the hydrogen column density ($N_{\rm H} = 4.8^{+3.3}_{-3.1} \times 10^{23}$ cm^{-2}) estimated with a torus model for Mrk 3 is consistent with the value derived from X-ray spectroscopy. The torus model geometry of Mrk 3 is similar to that of NGC 3281 (both are Compton-thick galaxies), confirmed through fitting the 9.7-μm silicate band profile. These results might provide further evidence that silicate-rich dust can be associated with the AGN torus and might also be responsible for the absorption observed at X-ray wavelengths in those galaxies.

Key words: techniques: spectroscopic – dust, extinction – ISM: molecules – galaxies: individual: Markarian 3 – galaxies: Seyfert – infrared: ISM.

1 INTRODUCTION

The currently favoured unified models of active galactic nuclei (AGNs) are orientation-based models, which propose that the differences between different classes of objects arise because of their different orientations to the observer. These models propose the existence of a dense concentration of absorbing material in their central engine in a toroidal distribution, which blocks the broad-line region (BLR) from the line of sight in type 2 objects (for reviews, see Antonucci 1993; Urry & Padovani 1995). However, a key issue with regards to the physics of AGNs, though not well understood, is the composition and nature of this dusty torus.

For example, several of these models predict that the silicate emission/absorption features at 9.7 and 18 μm are related to the observer's viewing angle, in the framework of the AGN unified model (e.g. Pier & Krolik 1992; Granato & Danese 1994; Granato, Danese & Franceschini 1997; Rowan-Robinson 1995; Nenkova, Ivezić & Elitzur 2002; Nenkova et al. 2008a,b; Schartmann et al. 2005, 2008; Dullemond & van Bemmel 2005; Fritz, Franceschini & Hatziminaoglou 2006; Hönig et al. 2006; Hönig & Kishimoto 2010; Stalevski et al. 2012; Heymann & Siebenmorgen 2012; Efstathiou et al. 2013, and references therein). The strengths of these features are sensitive to the dust distribution and could be direct evidence of a connection between mid-infrared (MIR) optically thick galaxies and Compton-thick AGNs (see Shi et al. 2006; Mushotzky, Done & Pounds 1993; Wu et al. 2009; Georgantopoulos et al. 2011). In fact, we fitted the silicate feature at 9.7 μm of the Compton-thick

★E-mail: dinalvaires@gmail.com

NGC 3281 (Sales et al. 2011), using the CLUMPY torus models (Nenkova et al. 2002, 2008a,b). We found that the hydrogen column density derived from silicate profile is similar to that derived from the X-ray spectrum originally employed to classify this galaxy as a Compton-thick source (see also Mushotzky et al. 1993; Shi et al. 2006; Thompson et al. 2009).

Such a result is further supported by the finding of Shi et al. (2006), who, using observations of the 9.7-μm silicate features in 97 AGNs, found that the strength of the silicate feature correlates with the H I column density estimated from fitting the X-ray data, with high and low H I columns corresponding to silicate absorption and emission, respectively. However, Thompson et al. (2009) suggested that even more informative than the 9.7-μm feature alone, the combination of this with the 18-μm silicate feature reveals the geometry of the reprocessing dust around the AGNs, discriminating between smooth and clumpy distributions (see also Sirocky et al. 2008). Moreover, comparing 31 type 1 Seyfert galaxy spectra obtained with the Infrared Spectrograph (IRS) onboard the *Spitzer Space Telescope* of 21 higher-luminosity quasi-stellar objects (QSOs), Thompson et al. (2009) have concluded that the weak emission lines observed are a consequence of clumpy AGN surroundings. In addition, when studying the 20 nearest bona fide Compton-thick AGNs using hard X-ray measurements, Goulding et al. (2012) have shown that only about half of the nearby Compton-thick AGNs have strong Si absorption features. They have concluded that not only is the dominant contribution to the observed MIR dust extinction related to the compact dusty obscuring structure surrounding the central engine, but also it can instead be originated from the host galaxy.

This paper is a part of a project to investigate the possibility that the presence of a silicate absorption feature at 9.7 μm would be the signature of a heavily obscured AGN. Here, we present a study of the nuclear spectrum of Mrk 3, an SB0 galaxy hosting an optically classified type 2 Seyfert galaxy (Sy 2) nucleus with a BLR detected in polarized light (Adams 1977; Miller & Goodrich 1990; Tran 1995; Collins et al. 2005). Capetti et al. (1995) have shown that the narrow-line region (NLR) of Mrk 3 has an S-shaped morphology, extended over nearly 2 arcsec, with a large number of resolved knots. They suggest that this morphology might be a consequence of the strong interaction between the NLR and the radio emission plasma (see Capetti et al. 1995; Ruiz et al. 2001; Schmitt et al. 2003a).

It is also known that Mrk 3 has a complex X-ray spectrum with heavily absorbed and cold reflection components, accompanied by a strong iron Kα line at ∼6.4 keV (Awaki et al. 1991, 2008; Turner et al. 1997; Cappi et al. 1999; Sako et al. 2000). Awaki et al. (2008) obtained an intrinsic 2–10 keV luminosity of $\sim 1.6 \times 10^{43}$ erg s^{-1}, and suggested it was direct emission from Mrk 3. In addition, they found that there is a heavily absorbed dust/gas component of $N_{\rm H} \sim 1.1 \times 10^{24}$ cm^{-2} obscuring the direct line of sight to the nucleus, which led them to classify Mrk 3 as a Compton-thick galaxy (see also Awaki et al. 1990, 1991; Iwasawa et al. 1994; Sako et al. 2000).

Nevertheless, there is some argument about the derived value of the hydrogen column density of Mrk 3, in the light of studies developed by Winter et al. (2009). They have shown that this target reveals a complex X-ray spectrum and a peculiar position in the colour–colour diagram of $F_{0.5-2\,\rm keV}/F_{2-10\,\rm keV}$ versus $F_{14-195\,\rm keV}/F_{2-10\,\rm keV}$, suggesting that it has a high column density with a complex irregular character (see Winter et al. 2009, for more details).

In this paper, we present ground-based, high spatial resolution, MIR spectra of the Compton-thick galaxy Mrk 3. Such observations allow the dust distribution to be studied in the central ∼200 pc of this galaxy. As stated above, the main goal is to investigate if the presence of a silicate absorption feature at 9.7 μm for Mrk 3 can be interpreted as a signature of a heavily obscured AGN caused by the dusty torus of the unified model. In addition, we briefly discuss the connection of the dusty torus material with the Compton-thick scattering material found in Sy 2 Mrk 3 and NGC 3281.

This paper is organized as follows. In Section 2, we briefly describe the observations and data reduction. In Section 3, we discuss the results, and we give concluding remarks in Section 5.

2 OBSERVATIONS AND DATA REDUCTION

Michelle is a MIR (7–26 μm) imager and spectrometer with a 320×240 pixels Si:As IBC array. When configured as a long-slit spectrometer, it has a plate scale of 0.183 arcsec pixel^{-1} and a 21.6 arcsec long slit. The low-resolution ($R \sim 200$) long-slit mode was used, with the two-pixel wide (0.366 arcsec) slit, resulting in a dispersion of 0.024 μm pixel^{-1} and a spectral resolution of 0.08 μm. The spectral coverage is ∼7 μm centred at 9.5 μm. The total on-source integration time was 10 min.

The data were obtained in queue mode at Gemini North, in 2010 February 05 UT, as part of programme GN-2009B-Q-61 (PI: M. Pastoriza). We obtained acquisition images with an on-source time of roughly 5 s through the *N*-band and Mrk 3 was observed under clear conditions (photometric/cloudless), with precipitable water vapour (PWV) in the range of 2.3 mm or less. The long-slit orientation and the extraction area of each spectrum are superposed upon the *N*-band acquisition and [O III] λ5007 Å (Schmitt et al. 2003b) images of Mrk 3 (Figs 1a and b). In Fig. 1(c), we also present the archive optical continuum image (F814W filter; programme 8645; PI: R. Windhorst) from the Wide Field and Planetary Camera 2 (WFPC2) onboard the *Hubble Space Telescope* (*HST*). The green box overplotted on this panel represents the field of view of 2.5 × 2.5 arcsec^2, and its amplification is shown in Fig. 1(d).

The image quality was measured from the *N*-band acquisition image of the telluric standard HD 45866 and turns out to be ∼0.7 arcsec (Fig. 2). In the same figure, we have also shown the spatial emission profile of Mrk 3 from two directions: north to south (dashed line) and east to west (dash-dotted line). Note that the spatial profile of the north–south (N–S) direction corresponds to our chosen position of Michelle's long slit (see Fig. 1). Both emission profiles, the N–S and east–west (E–W) directions, were normalized using the average flux of the two central pixels (0.366 arcsec) of Mrk 3.

A standard chop/nod technique was used to remove time-variable sky background, telescope thermal emission and the effect of 1/*f* noise from the array/electronics. The long slit was oriented along a position angle (PA) of 0°, with a chop throw of 15 arcsec, oriented along PA = 90°, which includes only the signal of the guided beam position in the frame and avoids possible nod effects in the spatial direction. The same slit position/nod orientations were used for the telluric standards.

Data reduction employed the MIDIR and GNIRS subpackages of the Gemini IRAF[1] package. The final spectrum was extracted from the combined chop- and nod-subtracted frames using the tasks TPREPARE

[1] IRAF is distributed by the National Optical Astronomy Observatory, which is operated by the Association of Universities for Research in Astronomy (AURA), Inc., under cooperative agreement with the National Science Foundation.

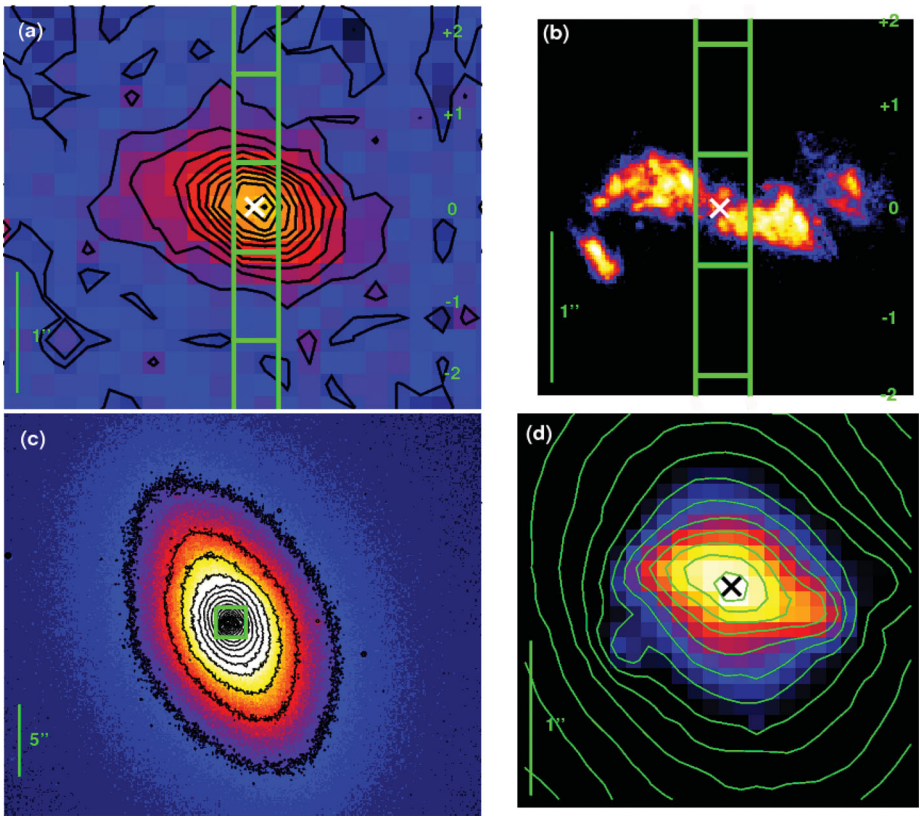

Figure 1. (a) The long-slit positions of Michelle overlaid on the contoured Mrk 3 acquisition image, which are linear and stepped at 5 per cent of the peak. (b) The [O III] λ5007 Å image of Mrk 3, which was observed using the Faint Object Camera (FOC) onboard the *HST*, taken from Schmitt et al. (2003b). The spectroscopic slits of Michelle are superposed. (c) The large-scale optical continuum (F814W filter) obtained from the *HST*/WFPC2 data archive (programme 8645; PI: R. Windhorst). The green box shows the central 2.5 × 2.5 arcsec^2 field of view. (d) The amplification of the green box shown in (c). The contours are logarithmically separated by a factor of 1.8. North is up and east is to the left. The positions of the nucleus, measured in the *HST*/F814W continuum images, are plotted as white and black crosses.

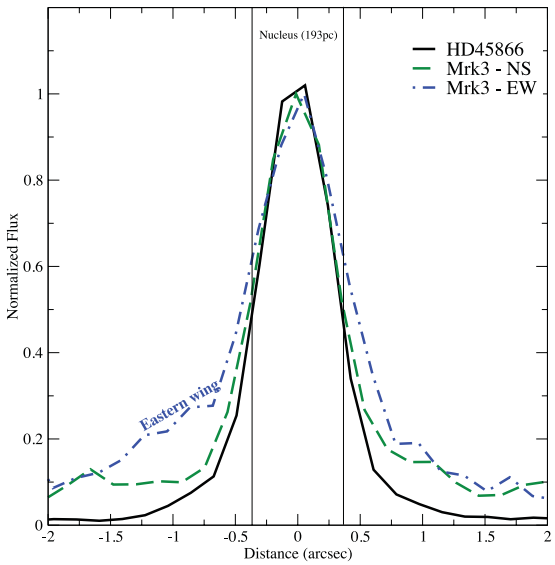

Figure 2. Spatial emission profile of Mrk 3 along the N–S (dashed line) and E–W (dash-dotted line) directions, compared with that of the telluric standard star (HD 45866, solid line). The fluxes were normalized to the peak value. The positions of each spectral extraction are labelled.

and MISTACK. Wavelength calibration was obtained from the skylines in the raw frames. Removal of the telluric absorption lines from the galaxy spectrum, and the flux calibration were performed using the MSTELLURIC task, selecting HD 45866 (Cohen et al. 1999) as the telluric standard, observed immediately after the science target.

As seen in Fig. 2, Mrk 3 has a luminosity profile similar to that of a point-like source, meaning that the bright AGN emission could dominate the total emission. However, there can be a contamination of an issuance arising from an extranuclear location. In light of this, we performed two extractions from the two-dimensional spectral image of Mrk 3, aiming to estimate the contribution of the host galaxy around the AGN.

Therefore, the first extraction was taken as the stellar FWHM (an aperture of four pixels or 0.732 arcsec, which corresponds to ∼193 pc for a distance of 55 Mpc, using $H_0 = 74$ km s^{-1} Mpc^{-1}), and the second is a spectrum of the whole emission available on Michelle's long slit (∼1 kpc). The host galaxy emission spectrum was derived by multiplying the central spectrum by a constant 1.314, further subtracting the result from the spectrum of the largest possible aperture. This accounts for the infinite aperture correction of the FWHM extraction of the Gaussian profile (see Ruschel-Dutra et al. 2014). We show in Fig. 3 both the nuclear and host galaxy spectra. The nuclear spectrum, an unresolved point-like source, was chosen to be centred at the peak of the continuum at ≈11.3 μm, which also coincides with the optical peak (see Fig. 1).

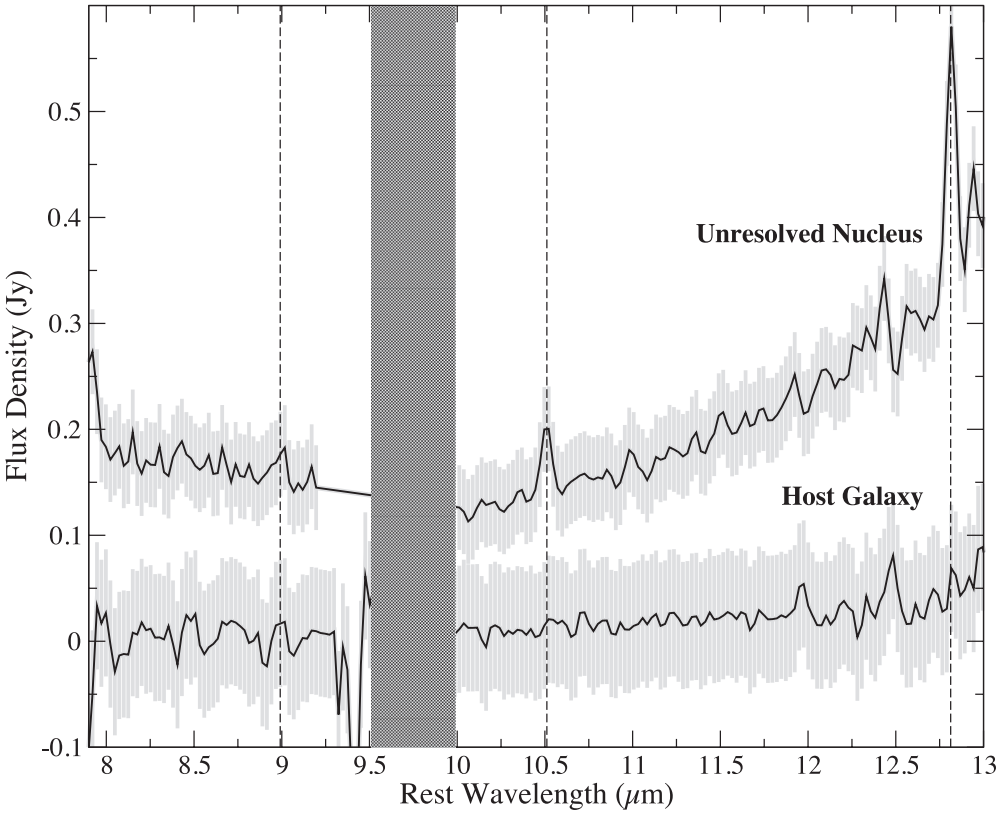

Figure 3. Spectra of the unresolved nucleus (0.732 arcsec or 193 pc) as well as the host galaxy of Mrk 3. Dotted lines show the [Ar III] 8.9 μm, [S IV] 10.5 μm and [Ne II] 12.8 μm ionic lines. The grey shaded area is the RMSD and the hatched area represents the O_3 telluric band.

The unresolved central spectrum of Mrk 3 clearly reveals the silicate absorption feature at 9.7 μm as well as prominent forbidden lines of [Ar III] 8.9 μm, [S IV] 10.5 μm and [Ne II] 12.8 μm, although the polycyclic aromatic hydrocarbon (PAH) emission is completely absent (Fig. 3). The corresponding spectrum of the host galaxy provides neither emission lines nor silicate features, however we can not draw any conclusive results due to the low S/N ratio.

3 RESULTS AND DISCUSSION

3.1 Acquisition image of Mrk 3: MIR emission in the NLR

As can be seen in Fig. 1(a), Mrk 3 shows resolved prominent wings with extended emission in a roughly E–W direction centred on the unresolved nucleus. This emission lobe has a PA of ∼70° and the easterly wing is extended within ∼1.5 arcsec, while the westerly minor knot is elongated to ∼0.7 arcsec. The emission in the N–S direction is unresolved with a FWHM similar to that of the telluric star, ≈0.7 arcsec. This might suggest that the bulk of emission perpendicular to the wing direction is dominated by the central unresolved bright source, implying that the putative torus could be the source of the central emission (see Section 4). However, we should note that the spatial resolution of the data is not sufficient to resolve the compact (<0.7 arcsec) point-like source on the N–S direction. This means that the torus emission could come from a smaller region, and thus we need data with higher spatial resolution to address this assumption.

Mrk 3 is a Sy 2 galaxy with a spectacular S-shaped NLR in the [O III] λ5007 Å emission image (Fig. 1). Its biconical region is extended towards ∼2 arcsec along the E–W direction and has been interpreted as the result of a rapid expansion of a cocoon of hot gas heated by radio emission (Capetti et al. 1995; Schmitt et al. 2003a). Curiously, our *N*-band acquisition image (Figs 1a and b) mimics a cylindrical shell aligned with the ionization cone of the [O III] λ5007 Å line. The same assumption can be drawn from the collapsed emission profile (Fig. 2) measured in the central 0.366 arcsec along the E–W direction. It is also notable that the eastern wing is the brightest and the most extended emission, 1 arcsec, of Mrk 3 at the *N*-band wavelength. Both the spatial position and open angle of this emission feature from the *N*-band coincide with the enhanced east wing present in the *HST* image of the [O III] λ5007 Å emission line.

The *N*-band emission structure is also spatially enclosed within the extended emission present in the optical continuum image of the *HST*/WFPC2 F814W filter (see Figs 1c and d). In order to highlight the extended NLR, we also overplotted contours on the optical continuum within the same field of view (2.5 × 2.5 arcsec^2) of the [O III] λ5007 Å image. The spatial coincidence of the extended MIR emission with the observed size of the high excitation emission region might suggest that the dust present in the NLR of Mrk 3 contributes to the *N*-band emission. Indeed, the dust located within the ionization cone, which might be heated by the central engine, can contribute to the emission at MIR wavelength, because this has been observed in several other AGNs (e.g. Radomski et al. 2002, 2003; Packham et al. 2005; Mason et al. 2006; Reunanen, Prieto & Siebenmorgen 2010).

In Table 1, we list the *N*-band flux density and surface brightness measured with the aperture for different radii (see Column 1). From these values, we can detected two regions of emitting dust. The brightest region arises from the central region at 0.366 arcsec

Table 1. *N*-band flux density of Mrk 3. The errors in the flux calibration are accurate to roughly 15 per cent according to Mason et al. (2006) and Packham et al. (2005).

Radius (arcsec)	Flux density (Jy)	Surface brightness (Jy arcsec^{-2})	Total flux (per cent)
0.366	0.21	0.51	36
0.732	0.44	0.26	73
1.098	0.55	0.15	91
1.464	0.59	0.09	97
1.83	0.60	0.06	100

(∼193 pc), which contributed 36 per cent of the total flux measured inside the radius of 1.83 arcsec, as well as the bulk of the *N*-band emission (surface brightness 0.51 Jy arcsec^{-2}; see Column 3 in Table 1). This result suggests that such a component, which dominates the unresolved point-like source, might emerge from the dusty torus predicted by the unified model (see also Radomski et al. 2002, 2003; Packham et al. 2005). We note that the spatial resolution used does not resolve the torus emission, and thus the silicate emission comes from the central 200 pc. However, it is clear that outside this region the emission of silicate, if it exists, is less than the detection limit of our Gemini/Michelle data.

The acquisition *N*-band image also shows a second component that is an extended diffuse emission with lower surface brightness extending up to 800 pc from the nucleus. This extended emission, which coincides with the NLR seen in the *HST* image of [O III] λ5007 Å (Fig. 1), is therefore probably a result of the dust emission located in the NLR and heated by the central source of Mrk 3.

3.2 Silicate absorption and emission-line measurements

According to Hao et al. (2007), the presence of the silicate absorption feature at 9.7 μm and no evidence of PAH emission bands could be interpreted as a galaxy with a heavily obscured active nucleus (see also Mushotzky et al. 1993; Shi et al. 2006; Thompson et al. 2009; Sales, Pastoriza & Riffel 2010; Sales et al. 2011, 2013). This scenario seems to be the case for our nuclear spectrum of Mrk 3 (Fig. 3), which presents a clear absorption feature at 9.7 μm, as well as strong ionic lines at [Ar III] 8.9 μm, [S IV] 10.5 μm and [Ne II] 12.8 μm, but no PAHs have been observed.

However, the high-resolution extended spectrum of Mrk 3, obtained with Gemini/Michelle, does not reveal such an increase in flux, setting not only a lower limit for the galactocentric distance of the dust emission observed by the *Spitzer*/IRS (see Weedman et al. 2005), but also corroborating the claim that the AGN torus of Mrk 3 is constrained within the central ∼200 pc extraction.

Following the procedure described by Spoon et al. (2007), we adjusted a liner continuum centred at 8 and 12.5 μm to derive the intrinsic, unobscured, AGN flux at 9.7 μm. From this, the apparent strength ($S_{\rm sil}$) of the silicate absorption has been calculated as

$$S_{\rm sil} = \ln \frac{f_{\rm obs}(9.7\,\mu{\rm m})}{f_{\rm cont}(9.7\,\mu{\rm m})}, \quad (1)$$

where $f_{\rm obs}$ and $f_{\rm cont}$ are the observed and the intrinsic AGN unobscured fluxes, respectively. Subsequently, we estimated the silicate optical depth, $\tau_{9.7}$, by the correlation of $\tau_{9.7} = -S_{\rm sil}$ (Nenkova et al. 2008b). The apparent optical extinction attributed to silicate dust can be inferred from $A_V^{\rm app} = \tau_{9.7} \times 18.5 \pm 2$ mag (Draine 2003). The resulting values are listed in Table 2.

We estimated a value of $S_{\rm sil} = -0.52 \pm 0.21$ for the unresolved nucleus of Mrk 3. This value is consistent with the average value observed in Sy 2 galaxies ($\langle S_{\rm sil} \rangle = -0.61$; see fig. 2 of Hao et al. 2007). From $S_{\rm sil}$, we derived an optical dust extinction of $A_V^{\rm app} = 9.6 \pm 0.51$ mag.

Table 2. Parameters derived from the MIR feature of Mrk 3. Fluxes are in units of 10^{-4} W m^{-2} sr^{-1}. Equivalent widths are in μm.

Features	λ (μm)	Centre
F [Ar III]	8.9	7.82 ± 1.9
EW [Ar III]	8.9	0.039
F [S IV]	10.5	7.60 ± 1.8
EW [S IV]	10.5	0.051
F [Ne II]	12.8	13.2 ± 2.5
EW [Ne II]	12.8	0.055
$S_{\rm sil}$	9.7	−0.52 ± 0.21
$A_V^{\rm app}$	–	9.6 ± 0.51
τ^a	9.7	1.46 ± 0.4
$A_V{}^a$	–	27 ± 0.4

[a]Values derived from the PAHFIT code.

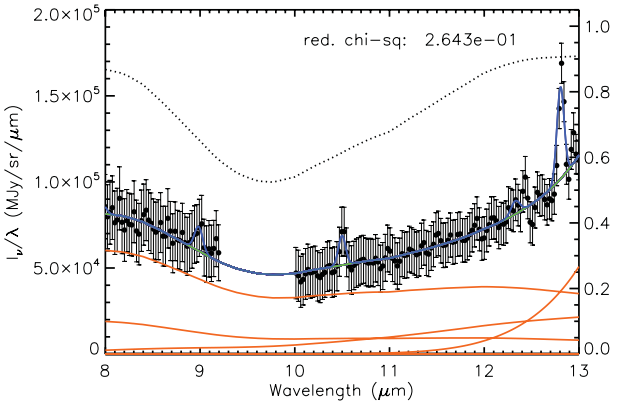

Figure 4. Decomposition of the centre spectrum of Mrk 3 using the PAHFIT code. The best-fitting model is represented by the blue line. The dotted black line indicates the mixed extinction components, while the orange lines represent the individual thermal continuum components.

In order to disentangle the contribution from each component in the spectral energy distribution (SED) of Mrk 3 as a function of the distance to the nucleus, we used the PAHFIT[2] IDL routines (Smith et al. 2007). This code decomposes the spectrum as continuum emission from dust and starlight, emission lines and individual and blended PAH emission bands, and it also assumes that the light is attenuated by extinction because of silicate grains. The code uses the dust opacity law of Kemper, Vriend & Tielens (2004), and the infrared extinction is considered as a power law plus silicate feature peaking at 9.7 μm.

The PAHFIT code requires information about the uncertainties, and here these have been assumed to be the root-mean-square deviation (RMSD) estimated from the whole spectral range of Michelle's *N*-band, presented as a grey shaded area in Fig. 3. Because the spectra do not show PAH emission, this component was not included in the fitting (see Sales et al. 2011). The resulting spectral decomposition of the nuclear extraction of Mrk 3 is shown in Fig. 4, and the fluxes derived to the emission lines are given in Table 2.

[2] The source code and documentation for PAHFIT are available at http://tir.astro.utoledo.edu/jdsmith/research/pahfit.php.

The unresolved nucleus shows $\tau_{9.7} = 1.46 \pm 0.4$. Inspecting the measured dust extinction (A_V) values obtained using PAHFIT, we can see that it is larger than those inferred from $S_{\rm sil}$. Such a difference arises because $S_{\rm sil}$ are obtained from the peak of the silicate feature at 9.7 μm, while the PAHFIT code takes into account the whole silicate profile (8–14 μm). Note that the optical depth values are similar to those found in other Seyfert galaxies (Gallimore et al. 2010).

4 DUSTY TORUS CONSTRAINTS FROM THE CENTRAL REGION OF MRK 3

In the unified model for AGNs, the presence of a nuclear toroidal structure composed by dust/gas-rich matter, mainly silicate and graphite, is postulated to attenuate the nuclear emission at ultraviolet/optical wavelengths and to re-emit it in the MIR, which leaves unmistakable signatures in the observed SEDs. While the sublimation of the graphite grains creates IR emission at $\lambda \geq 1$ μm, the ∼9.7-μm feature observed in emission/absorption is attributed to silicate grains (e.g. Barvainis 1987; Pier & Krolik 1992; Granato & Danese 1994; Siebenmorgen et al. 2005; Fritz et al. 2006; Rodríguez-Ardila & Mazzalay 2006; Riffel, Rodríguez-Ardila & Pastoriza 2006; Riffel et al. 2009). Some authors consider the torus to be a continuous density distribution (e.g. Pier & Krolik 1992; Granato et al. 1997; Siebenmorgen, Krügel & Spoon 2004; Fritz et al. 2006), but it has been postulated that, for dust grains to survive in the torus environment, they should be shielded within a clumpy structure (Krolik & Begelman 1988), which simultaneously provides a natural attenuation of the silicate feature (e.g. Nenkova et al. 2002, 2008a,b; Hönig et al. 2006).

As seen in Fig. 2, the emission profile within two central pixels (0.366 arcsec, the same width as Michelle's long slit) is quite similar to that of the telluric standard HD 45866. This shows that the dust emission in the NLR is not resolved at this spatial resolution. However, we can infer important information by modelling the emission from the unresolved nucleus. With this purpose, after masking the emission lines and the telluric band region (Fig. 3) using a simple interpolation, we subsequently compared the unresolved spectrum to CLUMPY[3] theoretical SEDs (Nenkova et al. 2002, 2008a,b). These models assume a complex clumpy dust distribution of the toroidal geometry of the AGN unified scheme, which is constrained by six parameters: (i) the number of dusty clouds along the torus equatorial ray, N_0; (ii) the visual optical depth of each clump, τ_V; (iii) the radial extension of the clumpy distribution, $Y = R_0/R_{\rm d}$, where R_0 and $R_{\rm d}$ are the outer and inner torus radii, respectively; (iv) the radial distribution of clouds as described by a power law $\propto r^{-q}$; (v) the torus angular width following a Gaussian angular distribution described by a half-width σ; (vi) the observer's viewing angle i.

In order to constrain the six torus parameters from the CLUMPY model, we used the BAYESCLUMPY tool developed by Asensio Ramos & Ramos Almeida (2009). Its statistic methodology is based on a Bayesian inference framework and performs a Markov chain Monte Carlo (MCMC) search over the parameter grid. This approach has become commonplace for SED fitting because of its economy and efficiency over an exhaustive search for large parameter spaces.

In order to describe the observed spectra, BAYESCLUMPY takes into account the first 13 eigenvectors of the principal component analysis, which is a very good representation of the whole $\sim 10^6$ model grid of the CLUMPY SED data base (see Asensio Ramos & Ramos Almeida 2009). The marginalized probability distributions are assessed as histograms of the Markov chain for each parameter derived from the automatic marginalization properties of the MCMC technique. We perform two running sets (Fig. 5), the first run used all six torus parameters as free, while the second run limited the observer's line-of-sight angle to be $i \geq 45^\circ$ (see Alonso-Herrero et al. 2011, for details). The stability of the solution has been confirmed by consecutive runs of the algorithm and the results are shown in Fig. 6 and Table 3.

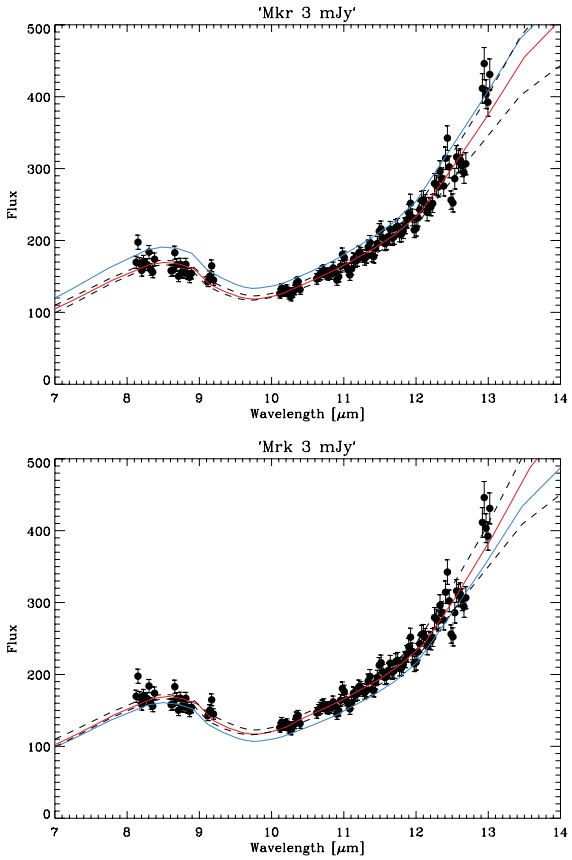

Figure 5. *N*-band fitting of Mrk 3 using a clumpy torus model. The blue line represents the best-fitting model taken from the values that maximize the probability distributions (MAP) of the parameters, while the red line describes the median value of each parameter. The dashed lines show the upper and lower limits of the 68 per cent confidence interval for each parameter around the median.

Following our approach, the CLUMPY model was able to reproduce very well the *N*-band spectrum of Mrk 3, using the observer view angle i as either a free parameter (first run) or fixed in the Sy 2 edge-on view (second run; see Fig. 5 and Table 3) predicted by the unified model of AGNs (Antonucci 1993). These modelling results show the presence of an embedded AGN surrounded by a dusty toroidal structure, constraining the radial thickness to $R_0/R_{\rm d} = 45^{+26}_{-18}$, i as free, or 38^{+25}_{-13} to the edge-on view. With the first run, it turned out that the torus of Mrk 3 has 9^{+3}_{-3} dusty clouds in its equatorial radius, with the individual clouds presenting an optical depth of $\tau_V = 93^{+10}_{-14}$ mag. The best fit on the second run was reached with 6^{+3}_{-1} clouds, with $\tau_V = 76^{+11}_{-12}$ mag instead.

Once we have forced the observer's line of sight to vary between 45° and 90°, following the assumption that an Sy 2 is always viewed close to the torus's plane, the i parameter becomes roughly 66^{+4}_{-13} deg, while when using i as a free parameter, we reached $i = 29^{+34}_{-17}$

[3] The models are available at http://www.pa.uky.edu/clumpy/.

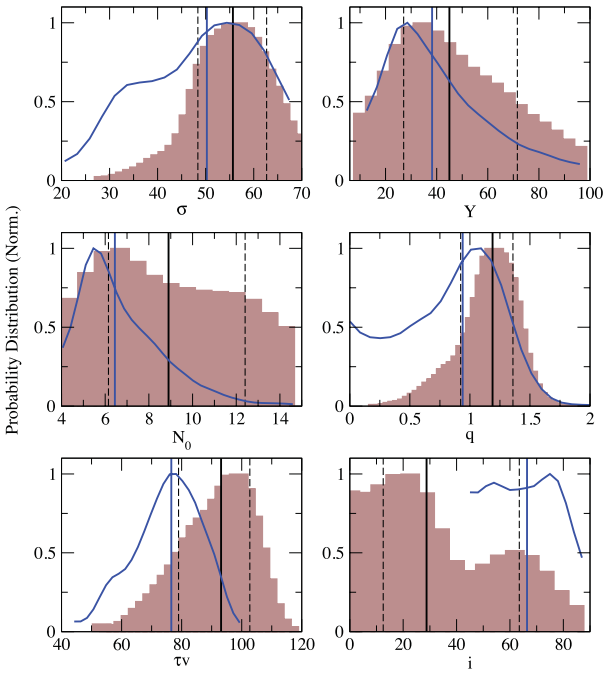

Figure 6. Probability distributions of the fitted parameters using Nenkova's clumpy torus model of Mrk 3 with the observer angle of view, *i*, taken as a free parameter (histograms) and constrained to be in the range $45^\circ \leq i \leq 90^\circ$ (blue curve). The solid lines, black and blue, represent the best models that maximize their probability distributions (MAP). The dashed lines indicate the 68 per cent confidence level for each parameter around the MAP. The marginal posterior distributions have been normalized to unity.

deg. The hydrogen column density along the observer's view is estimated by adopting a hydrogen column density of $N_{\rm H} \approx 10^{23}$ cm^{-2} (upper limit value) for each cloud (Nenkova et al. 2002, 2008a,b) and adopting the number of clouds over the observer's line of sight as

$$N_{\rm obs} = N_0 \exp\left[-\frac{(90-i)^2}{\sigma^2}\right]. \quad (2)$$

Table 3. CLUMPY torus parameters of Mrk 3.

Parameter	Best fit[a]	68 per cent confidence interval	
		Upper	Lower
Angular width (σ)	56°	48°	63
Radial thickness (Y)	45	27	71
Number of clouds (N_0)	9	6	12
Index of radial density (q)	1.18	0.92	1.35
Observer angle (i)	29°	12°	63°
Cloud optical depth (τ_V)	93 mag	79 mag	103 mag
Observer angle constrained as edge-on view ($45^\circ \leq i \leq 90^\circ$)			
Angular width (σ)	50°	35°	61°
Radial thickness (Y)	38	25	63
Number of clouds (N_0)	6	5	9
Index of radial density (q)	0.94	0.39	1.25
Observer angle (i)	66°	53°	70°
Cloud optical depth (τ_V)	76 mag	64 mag	87 mag

[a]The value parameters that maximizes their probability (MAP) distributions.

Table 4. Parameters derived from CLUMPY constraints.

Parameter	$0^\circ \leq i \leq 90^\circ$	$45^\circ \leq i \leq 90^\circ$
Bolometric luminosity, $L_{\rm bol}$ (erg s^{-1})	1.82×10^{44}	2.17×10^{44}
X-ray luminosity, $L_{\rm X\text{-}ray}$ (erg s^{-1})	9.1×10^{42}	1.35×10^{43}
Hydrogen column density, $N_{\rm H}^{\rm obs}$ (cm^{-2})	$2.7^{+7.2}_{-2.2} \times 10^{23}$	$4.8^{+3.3}_{-3.1} \times 10^{23}$
Direct view of AGN, $P_{\rm esc}$ (per cent)	6	0.85
Inner radius of torus, $R_{\rm d}$ (pc)	0.17	0.19
Outer radius of torus, R_0 (pc)	$7.68^{+4}_{-3.4}$	$7.08^{+5}_{-2.2}$

This leads to upper limit values of $N_{\rm H}^{\rm obs} = 2.7^{+7.2}_{-2.2} \times 10^{23}$ cm^{-2} and $4.8^{+3.3}_{-3.1} \times 10^{23}$ cm^{-2} using results from the first and second runs, respectively (see Fig. 6 and Table 4).

Using the equation (Nenkova et al. 2008b)

$$R_{\rm d} = 0.4 \times \left(\frac{1500\,{\rm K}}{T_{\rm sub}}\right)^{2.6} \left(\frac{L_{\rm bol}}{10^{45}\,{\rm erg\,s^{-1}}}\right)^{0.5} {\rm pc}, \quad (3)$$

and adopting a dust sublimation temperature of $T_{\rm sub} = 1500$ K, we obtained the torus size as roughly $8^{+4}_{-3.4}$ and $7^{+5}_{-2.2}$ pc from the first and second runs, respectively.

The scale amplitude of the CLUMPY model's best fit to the *N*-band observed spectrum gives the bolometric flux of the AGN. Thus, we derived a bolometric luminosity of $L_{\rm bol} = 1.82 \times 10^{44}$ erg s^{-1} for the first run and $L_{\rm bol} = 2.17 \times 10^{44}$ erg s^{-1} for the second run. In order to compare with X-ray observations, using a correction factor of 20 as proposed by Elvis et al. (2004), we converted these to the total X-ray luminosity, which reaches values of $L_{\rm X\text{-}ray} \approx 9.1 \times 10^{42}$ and $L_{\rm X\text{-}ray} \approx 1.35 \times 10^{43}$ erg s^{-1}, respectively.

4.1 Comparison with previous observations

We compare the parameters of the torus derived from the first and second runs with those obtained from X-rays observed by Awaki et al. (2008, 1990). The results obtained with the second run of Mrk 3, which fixed the edge-on torus view, are favoured (see Table 4) by the physical properties derived from X-ray observations. Indeed, the X-ray luminosity inferred from our modelling gives a similar value to that derived from the X-ray data (see Table 4). Using the X-ray high-quality wide-band (0.4–70 keV) spectrum of Mrk 3

observed with the *Suzaku* telescope, Awaki et al. (2008) were able to derive an intrinsic X-ray luminosity of $L_{2-10\,\mathrm{keV}} = 1.6 \times 10^{43}$ erg s^{-1} for this galaxy, concluding that it is quite completely attenuated by Compton-thick cold matter with $N_{\mathrm{H}} \sim 1.1 \times 10^{24}$ cm^{-2}. However, the clumpy torus model give us a hydrogen column density of $N_{\mathrm{H}}^{\mathrm{obs}} \sim 4.8^{+3.3}_{-3.1} \times 10^{23}$, about two times smaller than the value obtained by Awaki et al. (1990, 2008, $N_{\mathrm{H}} \sim 0.7$–1.1×10^{24} cm^{-2};). They also inferred the existence of a Compton shoulder to the iron Kα line, interpreted as the presence of a dusty torus. They also suggested that the iron emitting matter is located at >1 pc from the hidden nuclear engine. However, the size of the scattering region, because of the ionized gas, extends roughly over 50 pc (see also Awaki et al. 1990; Sako et al. 2000; Pounds & Page 2005; Serlemitsos et al. 2007).

We assume that the probability of a photon escaping from the central source towards the viewing angle i, in a clumpy environment composed by optically thick clouds ($\tau_V > 1$), is determined by $P \simeq \exp(-N_{\mathrm{obs}})$, where N_{obs} is the number of clouds in the observer's line of sight. The first and second runs yield $P \sim 6$ and $P \sim 0.85$ per cent, respectively. These results suggest that our run with the Sy 2 view recovers a scenario where the amount of ionizing photons from the AGN are absorbed by the torus cloud environment, as predicted by unified models. This might explain the Sy 2 optical features observed in this galaxy. However, it is difficult to set tight constraints from our modelling because not even the high-spatial resolution of the Gemini/Michelle *N*-band spectrum can spatially resolve the point-like source of Mrk 3 nor can it allow the contribution from dust in the host galaxy to be estimated (see Goulding et al. 2012).

4.2 Compton-thick torus model geometry of Sy 2: Mrk 3 and NGC 3281

In the clumpy dust torus model for AGN obscuration discussed above, the observed strength of the silicate dust features is expected to be dependent on the specific geometry and optical depth of the torus (Granato & Danese 1994; Nenkova et al. 2002; Fritz et al. 2006). In addition, the dust would be co-spatial with cold neutral gas, which absorbs the X-ray wavelength light from the AGN (see Mushotzky et al. 1993; Shi et al. 2006; Wu et al. 2009). In particular, Shi et al. (2006) found that the strength of the silicate feature correlates with the hydrogen column density, suggesting that the material surrounding the central engine is responsible for obscuring both the X-ray and the silicate emission. Therefore, Georgantopoulos et al. (2011) has postulated that the presence of a strong MIR silicate feature in absorption can be used as a good method to find the most heavily obscured AGNs, also called Compton-thick sources.

Following this direction, Sales et al. (2011) represented the torus model geometry of Compton-thick Sy 2 NGC 3281 using the CLUMPY models. They found evidence that the matter responsible for the silicate absorption at 9.7 μm could also be responsible for the X-ray scattering, with a column density of $N_{\mathrm{H}} \sim 1.2 \times 10^{24}$ cm^{-2}. We also constrained the parameters of the CLUMPY model to the torus geometry of Mrk 3 (see Section 4), which might indicate a similar correlation between the dusty material associated with the silicate feature and the X-ray scattering region in this galaxy. However, we should note that there might be some controversy with regards to this conclusion; it has been explored by Goulding et al. (2012) but needs to be addressed further. The physical parameters of each torus are listed in Table 5.

From our analysis, we can conclude that the torus model geometry derived for NGC 3281 and Mrk 3 are quite similar. The only differences are in the visual optical depth of the clump's clouds as well as the total number of clouds in the torus equatorial radius, suggesting that the dust torus in NGC 3281 is more compact than that of Mrk 3 (Table 5).

If we take

$$A_V^{\mathrm{obs}} = 1.086\, N_0\, \tau_V\, \exp\left[-\frac{(i-90)^2}{\sigma^2}\right]$$

as an estimate of the optical extinction along the line of sight, we obtain $A_V^{\mathrm{obs}} = 506$ mag for NGC 3281, and $A_V^{\mathrm{obs}} = 393$ mag for Mrk 3. The difference in the optical obscuration generated by the two tori might explain the depth of the silicate profiles, because the spectrum of NGC 3281 shows a deeper silicate feature than that of Mrk 3 (see fig. 2 in Sales et al. 2011). It is important to highlight that the comparison of the torus model geometries of Mrk 3 and NGC 3281 is not straightforward because the fitting methodology of the clumpy models used by Sales et al. (2011) is different from that used here.

Furthermore, we can estimate the density of silicate matter as

$$\rho_{9.7\,\mu\mathrm{m}} = \tau_{9.7\,\mu\mathrm{m}}/\kappa L, \tag{4}$$

where $\tau_{9.7\,\mu\mathrm{m}}$ was obtained from the PAHFIT analysis, κ is the mass absorption coefficient of the emitter material, and L is the length of the emitting region. Assuming $\kappa = 315$ m^2 kg^{-1}, which corresponds to $MgSiO_3$ amorphous silicate (see table 5 in Whittet 2003), and L to be the length of uncontaminated nuclear extraction (193 pc), we obtain $\rho_{9.7\,\mu\mathrm{m}} = 7.1 \times 10^{-21}$ and 7.8×10^{-22} kg m^{-3} for NGC 3281 and Mrk 3, respectively. This difference in the silicate density values is in agreement with the trend found for the optical extinction inferred using the SEDs of the CLUMPY models.

Note that the modelling of the silicate feature at 9.7 μm using the clump torus of Nenkova et al. (2002) also allows us to compare the hydrogen column density with the values derived from X-ray observations. Both NGC 3281 ($N_{\mathrm{H}} \approx 1.5 \times 10^{24}$ cm^{-2}) and Mrk 3 ($N_{\mathrm{H}} \approx 4.8^{+3.3}_{-3.1} \times 10^{23}$ cm^{-2}) have been classified as Compton-thick sources (see also Vignali & Comastri 2002; Awaki et al. 2008; Sales et al. 2011). Therefore, the results from Sales et al. (2011) and the new results presented here likely provide further evidence that the silicate-rich dust is indeed associated with the AGN torus and is possibly also responsible for the absorption observed at X-ray wavelengths. However, it is necessary to obtain higher spatial resolution from the data and to have further accuracy in its modelling.

Because Mrk 3 has a roughly face-on view ($b/a = 0.89$; Goulding et al. 2012), we have interpreted that the bulk of the *N*-band emission comes from a region less than the unresolved central ~200 pc. In addition, we are assuming that the dominant emission is related to the putative torus of the AGN unified model. However, despite our claim, the high spatial resolution (0.366 arcsec) of Gemini/Michelle is not enough to isolate the Mrk 3 torus emission from its inner 200 pc. Hence, we have to keep in mind that our nuclear spectrum might have a contribution of the silicate dust located in the inner 200 pc of the Mrk 3 bulge, as suggested for other galaxies (for reviews, see Deo et al. 2007, 2009; Goulding & Alexander 2009; Mullaney et al. 2011).

Moreover, Shi et al. (2006) have also suggested that the structure of the material surrounding the central black hole requires a multiphase medium composed of a circumnuclear disc geometry plus a middle disc with a diffuse component and embedded denser clouds, as well as the clumpy outer disc. Hence, we need to keep in mind that the direct relation of the dust-to-gas ratio, as we have used here, is causing concern. However, this issue is not within the scope of this paper and should be investigated more carefully in the future.

Table 5. Resulting parameters for the torus models of NGC 3281 and Mrk 3.

Parameter	NGC 3281	Mrk 3
Torus angular distribution width (σ)	70°	50°
Radial torus thickness (Y)	20	38
Clumps along to torus equatorial radius (N_0)	10	6
Power-law index of radial density (q)	1.0	0.94
Observer viewing angle (i)	60°	66°
Clump visual optical depth (τ_V)	40 mag	76 mag
Torus outer radii (R_0)	11 pc	7 pc
Observer visual extinction ($A_V^{\rm obs}$)	506 mag	393 mag
$MgSiO_3$ amorphous silicate density ($\rho_{9.7\,\mu m}$)	7.1×10^{-21}kg m^{-3}	7.8×10^{-22} kg m^{-3}
Observer column density ($N_{\rm H}$)	1.5×10^{24} cm^{-2}	4.76×10^{23} cm^{-2}
Nuclear extraction size	65 pc	193 pc

5 SUMMARY AND CONCLUSIONS

In this paper, we have presented a study using high spatial resolution (∼193 pc) spectra of the *N*-band wavelength (8–13 μm) of the well-known Compton-thick galaxy Mrk 3 in order to investigate the correlation between the Compton-thick material seen at X-ray wavelengths and the silicate grain signature at 9.7 μm. We also compare the results find here to Mrk 3 with those of Compton-thick galaxy NGC 3281, where the silicate absorption properties could be linked to Compton-thick material from X-ray spectra. Our main conclusions are as follows.

(i) No PAH emissions were detected in the Mrk 3 spectra. However, strong [Ar III] 8.9 μm, [S IV] 10.5 μm and [Ne II] 12.8 μm ionic emission lines as well as a silicate absorption feature at 9.7 μm have been detected at the nuclear spectrum.

(ii) By analysing the *N*-band image of Mrk 3, we are able to detect two emitting regions, the brightest of which is dominated by the unresolved central source that might emerge from the dusty torus of the unified model. However, we should note that the spatial resolution of our Gemini/Michelle spectrum could not actually resolve the nuclear torus emission. The second component is an extended MIR emission from the circumnuclear region of Mrk 3. This diffuse dust emission shows up as a wing towards the E–W direction, mimicking the same S-shape of the NLR as has been seen in the optical image of [O III] λ5007 Å.

(iii) The nuclear spectrum was compared with $\sim 10^6$ SEDs of CLUMPY torus models. The result suggests that the nuclear region of Mrk 3 hosts a dusty toroidal structure with an angular cloud distribution of $\sigma = 50^{+11}_{-15}$ deg, an observer's view angle $i = 66^{+4}_{-13}$ deg and an outer radius of $R_0 \sim 7^{+5}_{-2.2}$ pc. The hydrogen column density along the line of sight, derived from the torus models of Nenkova, is $N_{\rm H} = 4.8^{+3.3}_{-3.1} \times 10^{23}$ cm^{-2}. The torus models also provide an estimate for the X-ray luminosity ($L_{\rm X\text{-}ray} \approx 1.35 \times 10^{43}$ erg s^{-1}) of the AGN in Mrk 3 and this value is comparable to that derived from observed X-ray spectra, $L = 6.2 \times 10^{43}$ erg s^{-1}.

(iv) By comparing the torus properties of Mrk 3 and NGC 3281 Compton-thick Sy 2 galaxies, we obtain similar torus model geometries. This result perhaps indicates further evidence that the silicate dust is associated with the torus predicted by the unified model of AGNs, and could also be responsible for the absorption observed at the X-ray wavelengths of those galaxies classified as Compton-thick sources. However, it is necessary to obtain better spatial resolution in order to address this assumption.

ACKNOWLEDGEMENTS

MGP would like to acknowledge support from CNPq (grant 308985/2009-5). RR acknowledges funding from FAPERGs (ARD 11/1758-5) and CNPq (grant 304796/2011-5). This work is based on observations obtained at the Gemini Observatory, which is operated by the Association of Universities for Research in Astronomy, Inc., under a cooperative agreement with the National Science Foundation (NSF) on behalf of the Gemini partnership: the NSF (United States), the Science and Technology Facilities Council (United Kingdom), the National Research Council (Canada), CONICYT (Chile), the Australian Research Council (Australia), Ministério da Ciência e Tecnologia (Brazil) and Ministerio de Ciencia, Tecnología e Innovación Productiva (Argentina).

REFERENCES

Adams T. F., 1977, ApJS, 33, 19
Alonso-Herrero A. et al., 2011, ApJ, 736, 82
Antonucci R., 1993, ARA&A, 31, 473
Asensio Ramos A., Ramos Almeida C., 2009, ApJ, 696, 2075
Awaki H., Koyama K., Kunieda H., Tawara Y., 1990, Nature, 346, 544
Awaki H., Koyama K., Inoue H., Halpern J. P., 1991, PASJ, 43, 195
Awaki H. et al., 2008, PASJ, 60, 293
Barvainis R., 1987, ApJ, 320, 537
Capetti A., Macchetto F., Axon D. J., Sparks W. B., Boksenberg A., 1995, ApJ, 448, 600
Cappi M. et al., 1999, A&A, 344, 857
Cohen M., Walker R. G., Carter B., Hammersley P., Kidger M., Noguchi K., 1999, AJ, 117, 1864
Collins N. R., Kraemer S. B., Crenshaw D. M., Ruiz J., Deo R., Bruhweiler F. C., 2005, ApJ, 619, 116
Deo R. P., Crenshaw D. M., Kraemer S. B., Dietrich M., Elitzur M., Teplitz H., Turner T. J., 2007, ApJ, 671, 124
Deo R. P., Richards G. T., Crenshaw D. M., Kraemer S. B., 2009, ApJ, 705, 14
Draine B. T., 2003, ARA&A, 41, 241
Dullemond C. P., van Bemmel I. M., 2005, A&A, 436, 47
Efstathiou A., Christopher N., Verma A., Siebenmorgen R., 2013, MNRAS, 436, 1873
Elvis M., Risaliti G., Nicastro F., Miller J. M., Fiore F., Puccetti S., 2004, ApJ, 615, L25
Fritz J., Franceschini A., Hatziminaoglou E., 2006, MNRAS, 366, 767
Gallimore J. F. et al., 2010, ApJS, 187, 172
Georgantopoulos I. et al., 2011, A&A, 531, A116
Goulding A. D., Alexander D. M., 2009, MNRAS, 398, 1165

Goulding A. D., Alexander D. M., Bauer F. E., Forman W. R., Hickox R. C., Jones C., Mullaney J. R., Trichas M., 2012, ApJ, 755, 5
Granato G. L., Danese L., 1994, MNRAS, 268, 235
Granato G. L., Danese L., Franceschini A., 1997, ApJ, 486, 147
Hao L., Weedman D. W., Spoon H. W. W., Marshall J. A., Levenson N. A., Elitzur M., Houck J. R., 2007, ApJ, 655, L77
Heymann F., Siebenmorgen R., 2012, ApJ, 751, 27
Hönig S. F., Kishimoto M., 2010, A&A, 523, A27
Hönig S. F., Beckert T., Ohnaka K., Weigelt G., 2006, A&A, 452, 459
Iwasawa K., Yaqoob T., Awaki H., Ogasaka Y., 1994, PASJ, 46, L167
Kemper F., Vriend W. J., Tielens A. G. G. M., 2004, ApJ, 609, 826
Krolik J. H., Begelman M. C., 1988, ApJ, 329, 702
Mason R. E., Geballe T. R., Packham C., Levenson N. A., Elitzur M., Fisher R. S., Perlman E., 2006, ApJ, 640, 612
Miller J. S., Goodrich R. W., 1990, ApJ, 355, 456
Mullaney J. R., Alexander D. M., Goulding A. D., Hickox R. C., 2011, MNRAS, 414, 1082
Mushotzky R. F., Done C., Pounds K. A., 1993, ARA&A, 31, 717
Nenkova M., Ivezić Ž., Elitzur M., 2002, ApJ, 570, L9
Nenkova M., Sirocky M. M., Ivezić Ž., Elitzur M., 2008a, ApJ, 685, 147
Nenkova M., Sirocky M. M., Nikutta R., Ivezić Ž., Elitzur M., 2008b, ApJ, 685, 160
Packham C., Radomski J. T., Roche P. F., Aitken D. K., Perlman E., Alonso-Herrero A., Colina L., Telesco C. M., 2005, ApJ, 618, L17
Pier E. A., Krolik J. H., 1992, ApJ, 401, 99
Pounds K. A., Page K. L., 2005, MNRAS, 360, 1123
Radomski J. T., Piña R. K., Packham C., Telesco C. M., Tadhunter C. N., 2002, ApJ, 566, 675
Radomski J. T., Piña R. K., Packham C., Telesco C. M., De Buizer J. M., Fisher R. S., Robinson A., 2003, ApJ, 587, 117
Reunanen J., Prieto M. A., Siebenmorgen R., 2010, MNRAS, 402, 879
Riffel R., Rodríguez-Ardila A., Pastoriza M. G., 2006, A&A, 457, 61
Riffel R., Pastoriza M. G., Rodríguez-Ardila A., Bonatto C., 2009, MNRAS, 400, 273
Rodríguez-Ardila A., Mazzalay X., 2006, MNRAS, 367, L57
Rowan-Robinson M., 1995, MNRAS, 272, 737
Ruiz J. R., Crenshaw D. M., Kraemer S. B., Bower G. A., Gull T. R., Hutchings J. B., Kaiser M. E., Weistrop D., 2001, AJ, 122, 2961
Ruschel-Dutra D., Pastoriza M., Riffel R., Sales D. A., Winge C., 2014, MNRAS, 438, 3434
Sako M., Kahn S. M., Paerels F., Liedahl D. A., 2000, ApJ, 543, L115
Sales D. A., Pastoriza M. G., Riffel R., 2010, ApJ, 725, 605
Sales D. A., Pastoriza M. G., Riffel R., Winge C., Rodríguez-Ardila A., Carciofi A. C., 2011, ApJ, 738, 109
Sales D. A., Pastoriza M. G., Riffel R., Winge C., 2013, MNRAS, 429, 2634
Schartmann M., Meisenheimer K., Camenzind M., Wolf S., Henning T., 2005, A&A, 437, 861
Schartmann M., Meisenheimer K., Camenzind M., Wolf S., Tristram K. R. W., Henning T., 2008, A&A, 482, 67
Schmitt H. R., Ulvestad J. S., Antonucci R. R. J., Kinney A. L., 2003a, ApJS, 132, 199
Schmitt H. R., Donley J. L., Antonucci R. R. J., Hutchings J. B., Kinney A. L., 2003b, ApJS, 148, 327
Serlemitsos P. J. et al., 2007, PASJ, 59, 9
Shi Y. et al., 2006, ApJ, 653, 127
Siebenmorgen R., Krügel E., Spoon H. W. W., 2004, A&A, 414, 123
Siebenmorgen R., Haas M., Krügel E., Schulz B., 2005, A&A, 436, L5
Sirocky M. M., Levenson N. A., Elitzur M., Spoon H. W. W., Armus L., 2008, ApJ, 678, 729
Smith J. D. T. et al., 2007, ApJ, 656, 770
Spoon H. W. W., Marshall J. A., Houck J. R., Elitzur M., Hao L., Armus L., Brandl B. R., Charmandaris V., 2007, ApJ, 654, 49
Stalevski M., Fritz J., Baes M., Nakos T., Popović L. Č., 2012, MNRAS, 420, 2756
Thompson G. D., Levenson N. A., Uddin S. A., Sirocky M. M., 2009, ApJ, 697, 182
Tran H. D., 1995, ApJ, 440, 565
Turner T. J., George I. M., Nandra K., Mushotzky R. F., 1997, ApJS, 113, 23
Urry C. M., Padovani P., 1995, PASP, 107, 803
Vignali C., Comastri A., 2002, A&A, 381, 834
Weedman D. W. et al., 2005, ApJ, 633, 706
Whittet D. C. B., 2003, Dust in the Galactic Environment, 2nd edn. Institute of Physics Publishing, Bristol
Winter L. M., Mushotzky R. F., Reynolds C. S., Tueller J., 2009, ApJ, 690, 1322
Wu Y., Charmandaris V., Huang J., Spinoglio L., Tommasin S., 2009, ApJ, 701, 658

This paper has been typeset from a TEX/LATEX file prepared by the author.